CHAPTER 4
METHODS OF EVALUATION AND COMPARISON

4.1 Introduction

The purpose of this chapter is to describe the methods used to evaluate the data obtained from the field testing by VTRC. The specific load cases and data acquisition instruments used for evaluating the four scopes (load distribution, dynamic load allowance, composite action, and deck stresses developed) are included. In addition, the approximate methods employed by AASHTO SSHB (1996) and AASHTO LRFD (1994) for calculation of the load distribution and dynamic load allowance are presented. The "lever method" for load distribution was employed in the design calculations of the Little Buffalo Creek Bridge. The "lever method" is discussed more thoroughly in the load distribution section.

4.2 Elimination of Extraneous Data

It is common for plots of field data (i.e., strain versus time for a truck crossing) to show vibratory cycles that oscillate around the static response. In bridge testing, the vibratory cycles are often a result of high frequency cyclic loads that are caused by vehicle-bridge interaction. For instance, the bridge's approach surface contains irregularities that cause a vehicle's tires and suspension to bounce, resulting in vibratory loads.

Data collected from the deck gauges of various dynamic and pseudo-static load cases contained constant, electronic signal noise and/or cyclic signal noise that were not vibratory related; therefore, correction techniques were employed to get rid of the extraneous data. The deck gauges were wired to terminal blocks placed on the underside of the aluminum deck. The cause of the signal noise is believed to be a result of the wiring system from the terminal blocks to the data acquisition system, which was found to have been made with two wires rather than the usual three. The deck gauges were affected in Test Sets 2 and 3. Figure 4.1a, following this section, shows an original plot of

strain versus time for deck gauge TS-3 from Load Case 6 (Test Set 2) that contains constant, electronic signal noise. In addition, Figure 4.1b following this section shows a plot of strain versus time for transverse deck gauge TS-4 of Load Case PS-1 (Test Set 3) that contains constant, electronic signal noise and cyclic signal noise.

A "moving average" method was suggested by VTRC and employed to "smooth" the deck gauge data and remove the constant, electronic signal noise present in the field data. The actual method used was a "moving average of six." The data was averaged in sets of six with the data point sequence being 1-6, 2-7, 3-8, etc. until the end was reached. Table 4.1, following this section, shows values that result from applying a "moving average of six" to a set of seven original data points, and the resulting averaged data.

Based on the field data collected by VTRC, the constant, electronic signal noise present in the deck gauges was generally less than ± 5 micro-strains (με); however, two deck gauges had constant signal noise that were above ± 5 με. In Test Set 2, gauge TS 3 had constant signal noise of approximately ± 7 με, and gauge TS 2 had constant signal noise of nearly ± 29 με. The effect of applying a "moving average of six" caused the peak values of strain to drop in magnitude, while the shape of the strain response remained the same. The percent difference between the original data peaks and the moving average data peaks varied considerably amongst the gauges. In general the highest percent differences were for gauges that had low magnitudes of strain (i.e., less than 20 με) and/or gauges that experienced several strain reversals during recorded data. On average, the longitudinal deck gauges had the greatest number of strain reversals within the strain responses.

The cyclic signal noise shown in Figure 4.1b that appeared in the deck gauge data from Test Set 3 was removed by locating the data points and replacing them with an average value of the four data points before and the four data points after the cyclic signal data. This method was chosen over simply deleting the data points because it would allow for a moving average to be taken without adding in values of zero. The cyclic signal noise present within the pertinent data affected four data point or less at each cycle of occurrence. Because the data was sampled at a rate of 1/200 seconds, four cyclic data

points correspond to only 0.02 seconds. The removal of the cyclic data from the deck gauge samplings was done before the "moving average of six" was applied.

Figures 4.2a and 4.2b, following this section, show the plots that result from the application of the above procedures to eliminate the extraneous data in the deck gauges. Various mid span deflectometers within the dynamic load cases also contained constant, electronic signal noise that was removed. The magnitude of the constant, electronic signal noise present in the deflection data was extremely low (less than 0.005), but often the magnitude of deflection measured at certain girders was low (less than .03 inches). A "moving average of six" was applied to these girders, and to be consistent the moving average was applied to the deflection data of all girders. The effect of applying a moving average affected the peak deflection values of the most heavily loaded girders by less than six percent.

Table 4.1 Example Table of "Moving Average of Six"

Data Point #	Orig. Time	Orig. Data
1	1.245	79.78
2	1.250	100.41
3	1.255	57.44
4	1.260	53.84
5	1.265	95.73
6	1.270	70.09
7	1.275	66.56

Averaged Data Points	Moving Avg. Time	Moving Avg. Data
1-6	1.258	76.22
2-7	1.263	74.01

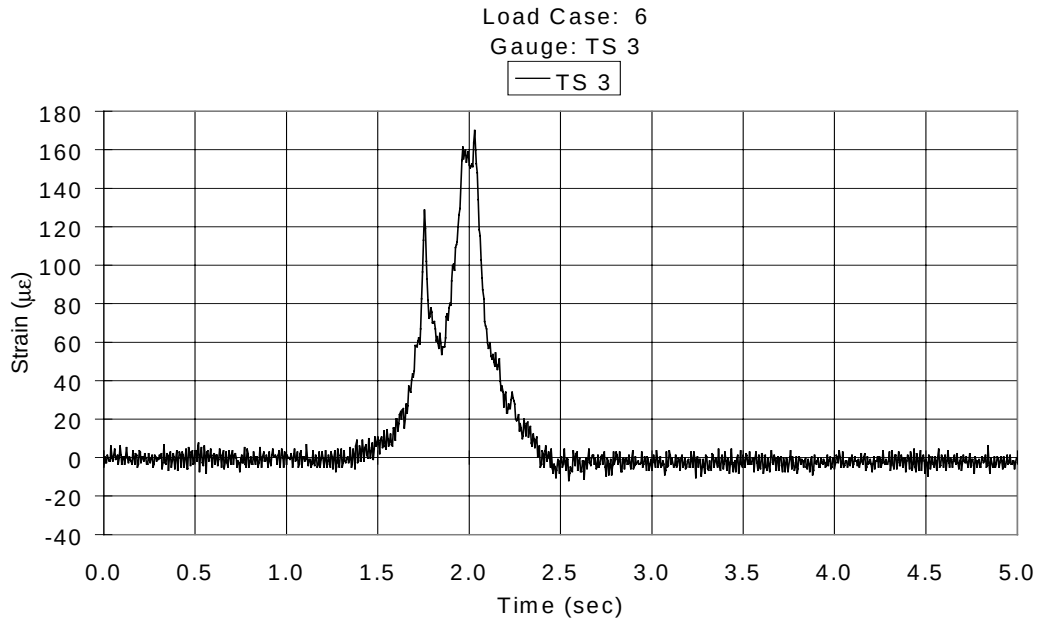

(a)

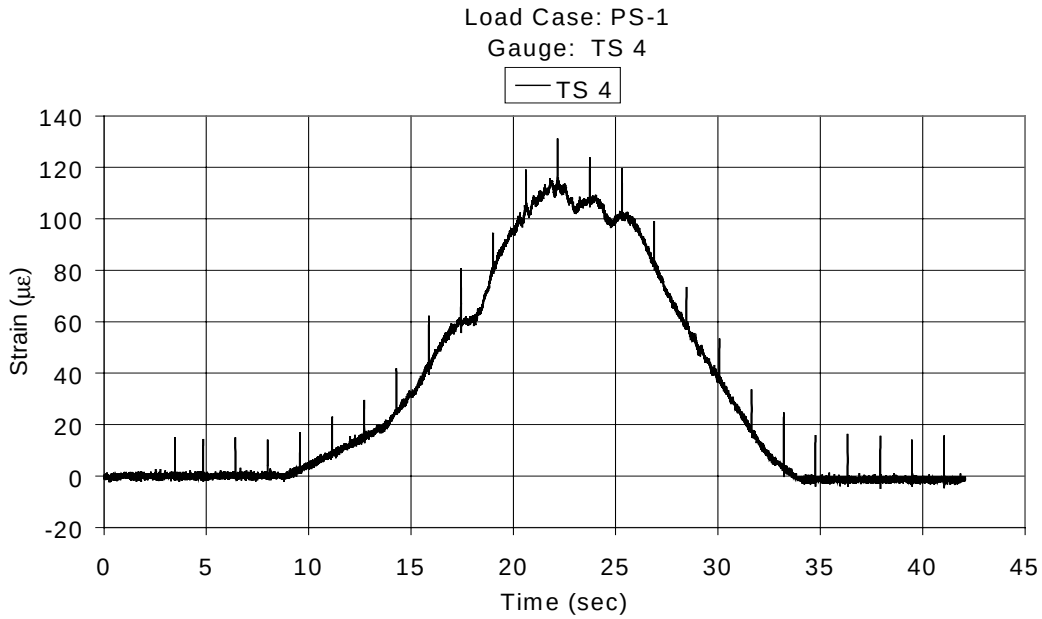

(b)

Figure 4.1 Deck Gauges with Electronic Signal Noise: (a) constant noise, and (b) cyclic and constant noise

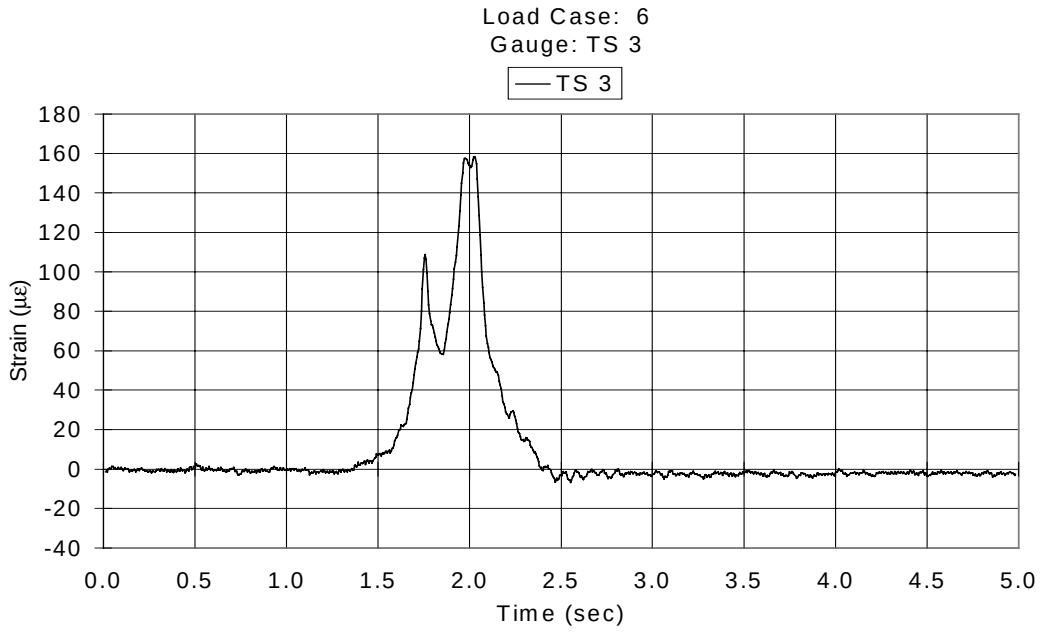

(a)

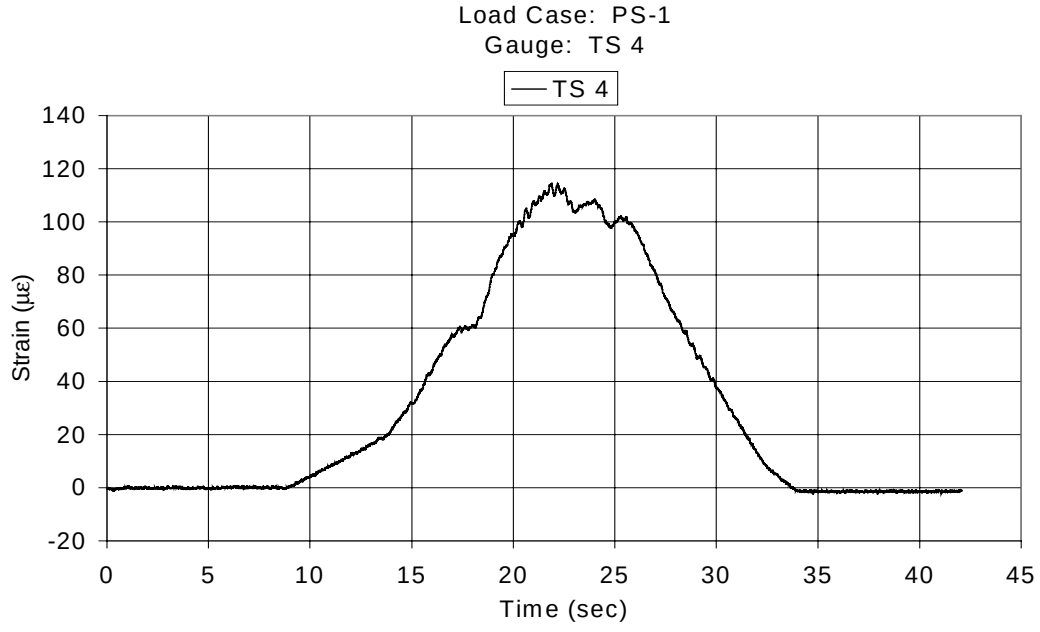

(b)

Figure 4.2 Deck Gauge Responses after Applying Correction Methods

4.3 Composite Action

4.3.1 Introduction

The Little Buffalo Creek Bridge was designed using full composite section properties. The grouted connection described in Chapter 3 was designed to provide for full composite action. Because this type of connection is new and rather unique in bridge design, the field data collected by VTRC was examined to attempt to determine the extent of composite action present between the girders and the deck. The composite behavior of the girders was evaluated for the stationary static load cases, Load Cases 1 and 2, and the pseudo-static load cases, PS-1 and PS-2. The evaluation consisted of developing a curve plotting the location of the neutral axis versus percent composite action. The curve was used along with the determined location of the neutral axis from the field data to attempt to quantify the level of composite action present.

4.3.2 Non-composite and Full Composite Section Properties

The non-composite section properties are the same for all girders because each plate girder has the same cross section. The discussion in Section 3.2.1.3 contains specific plate sizes for the plate girders. Appendix A (p.138) shows the calculation of the non-composite section properties, and Table 4.2 shows the calculated values.

Full composite section properties were determined using a transformed section approach. The effective flange widths, b_{eff}, were determined using both AASHTO SSHB (1996) and AASHTO LRFD (1994) for interior and exterior girders (Appendix A p. 139-143). The procedures used in the two specifications are slightly different and the effective width values differ by approximately five-percent for interior girders and four-percent for exterior girders, as shown in Table 4.3. The grouted cores of the deck-to-girder connection were considered to form solid rectangles 12 in. wide by 8 in. deep. The actual area of aluminum extrusion present within the grouted core was reduced from the effective deck area accordingly. In addition, the haunch was included in the transformed section analysis. The haunch depth was taken as the average haunch depth (h_{avg} = 2.75 in.) at mid-span measured from the Little Buffalo Creek Bridge. Table 4.3 shows the

neutral axis locations measured from the bottom of the steel girder and the top of the deck and the bottom section modulus for interior and exterior girders. The exterior girder section properties shown do not include the stiffening effects of the parapet. The percent differences in the full composite bottom section modulus values using AASHTO SSHB (1996) and AASHTO LRFD (1994) are below one-percent. In addition, the percent differences between interior and exterior girder, bottom section modulus values are below one-percent. Hence, the neutral axis location (y_b) and bottom section modulus (S_b) values are taken as the AASHTO SSHB (1996) values for all girders throughout the remainder of this paper.

Table 4.2 Non-composite Section Properties

Non-composite Section Properties		
y_t (in.)	y_b (in.)	S_b (in^3)
18.9	17.1	401.78

Table 4.3 Full Composite Section Properties

Full Composite Section Properties					
Girder Type	Specification	b_{eff} (ft)	y_t (in.)	y_b (in.)	S_b (in^3)
Interior	SSHB (1996)	8.00	13.4	33.4	624
	LRFD (1994)	8.44	13.2	33.6	626
	% Difference	5.4 %	1.7 %	0.7 %	0.4 %
Exterior	SSHB (1996)	7.50	13.7	33.1	621
	LRFD (1994)	7.22	13.8	32.9	620
	% Difference	3.8 %	1.2 5	0.5 %	0.3 %

4.3.3 Determination of Composite Action Curve

True non-composite behavior between a steel girder and slab results in independent behavior between the two elements. In essence, the steel girder acts alone in resisting the bending moment, and the section properties of the naked steel girder are used to determine the bending stresses for the non-composite scenario. Full composite

behavior results in the slab and girder acting as an entire unit to resist the bending moment, and thus the transformed section properties of the full composite slab and steel section are used to determine the bending stresses. The non-composite and full composite scenarios bound partial composite action, and the partial composite, neutral axis location lies between the non-composite and full composite neutral axis locations.

In the derivation of the composite action curve (Figure 4.4), the interface shear, Vc, was defined as the net compressive force required in the slab to balance the net tensile force in the steel girder. It was assumed that the location of the resultant of the compressive force in the slab would be in the same location despite the level of composite action occurring. The interface shear was placed at the top of the steel girder (i.e., at the interface of the girder top flange and haunch). Full composite action was defined using the transformed section properties of the aluminum deck and steel girder discussed in the previous section, and the full composite interface shear (~~V~~c) was the largest Vc possible. Non-composite action involved the steel girder acting alone, and results in the minimum Vc of zero.

The steps taken to derive the equations used in developing the composite action graph are presented here and the actual equations and excerpts of spreadsheet calculations are contained in Appendix A. The steps were as follows:

1) Calculate the moment required causing stress in the non-composite steel girder to be no larger than 25 ksi (1/2 Fy). This assures elastic behavior in the non-composite section. (Appendix A, p. 146)
2) Apply the moment from Step 1 to the full composite section and determine the stresses at the extreme outer fibers of the top flange and bottom flange of the steel girder. {Note: The small stresses at the top flange have associated small strains. Using a linear strain distribution and vertical interpolation, it is obvious that the stresses that would result in the grouted connection and the aluminum deck are elastic stresses.} (Appendix A, p. 146)
3) Using the stress distribution of the steel girder, determine the net tensile force present in the full composite girder. The compressive force required above the steel girder to balance the net tensile force in the steel is defined as the maximum interface shear (~~V~~c). (Appendix A, p. 146-148)
4) Sum moments about the extreme top fiber of the top flange of the steel plate girder, which is also the location of ~~V~~c. Define the resulting moment as the value ~~M~~c. (Appendix A, p. 148)

5) Place ~~M~~c on the composite girder with unknown neutral axis location, unknown interface shear (Vc), and thus unknown level of composite action. (Appendix A, p. 148)
6) Using a generic stress diagram of the steel girder with the applied moment of ~~M~~c and unknown interface shear of Vc, write two generic equations of equilibrium by summing forces and moments. The two equations can be manipulated to contain three unknowns: the extreme bottom flange outer fiber stress (σ_1), the location of the neutral axis from the bottom flange of the steel (y_b), and the percent composite action. (Appendix A, p. 149-150)
7) Using a spreadsheet, assume values of y_b between non-composite and full composite behavior and determine the associated values of bottom flange stress, σ_1. The complete stress diagram of the steel girder is now known because the values of σ_1 and y_b are known., and the stresses are elastic. (Appendix A, p. 150)
8) Using the generic equation from summation of forces, calculate the value of Vc required to balance the net tensile force in the steel girder. The ratio of Vc to ~~V~~c is the percent composite action. (Appendix A, p. 150)
9) Plot the location of the neutral axis, y_b, versus the percent composite action , ratio of Vc to ~~V~~c. (Appendix A, p. 150)

The stress diagrams and interface shear values for non-composite action, 50 percent composite action, and full composite action from the derivation are shown in Figure 4.3. Figure 4.4 shows the percent composite curve.

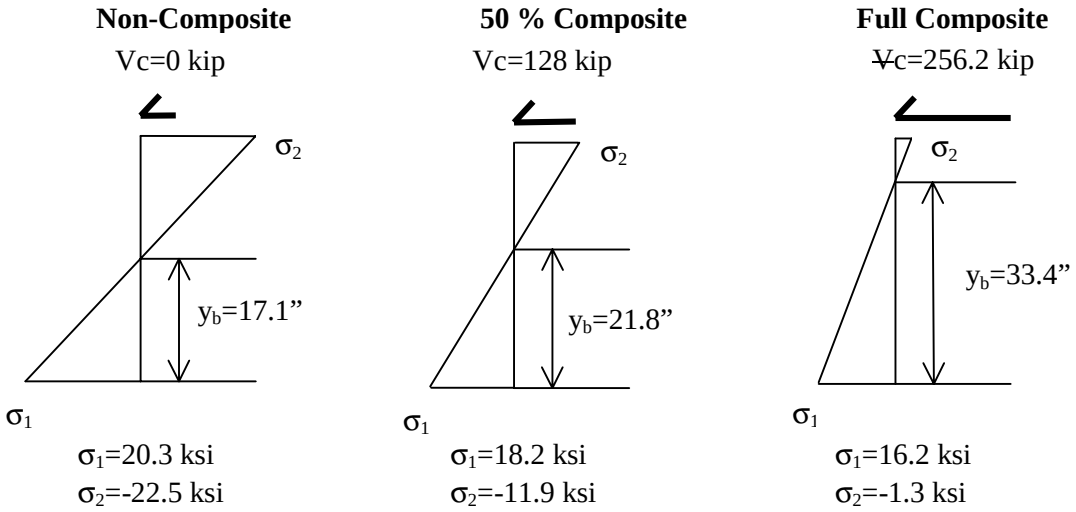

Figure 4.3 Various Percent Composite Stress Diagrams

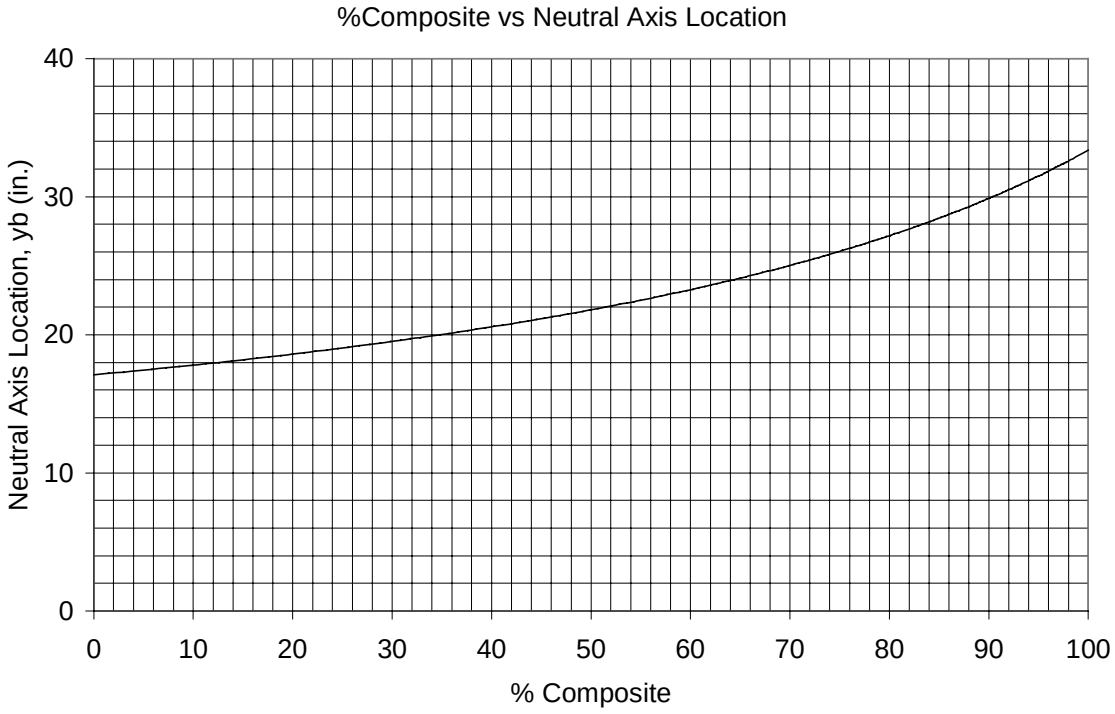

Figure 4.4 Percent Composite Curve

4.3.4 Neutral Axis Location from Field Data

The field data collected by VTRC was evaluated to determine the location of the neutral axis of interior and exterior girders. A linear strain distribution through the steel plate girder depth was used. The data from the bottom flange and top flange WIM gauges provided the necessary strains to determine the neutral axis locations. Stationary static load cases, Load Cases 1and 2, and pseudo-static load cases, Load Cases PS-1 and PS-2, were used to evaluate the composite action of the Little Buffalo Creek Bridge.

The neutral axis locations from the field data were then used in conjunction with the percent composite graph previously generated to determine the percent composite action present for the various load cases.

4.4 Load Distribution

4.4.1 Introduction

The load distribution behavior amongst the girders was evaluated for various static and dynamic load cases within the test sets. The data was evaluated to determine the effects of truck position (longitudinal and transverse) and truck speed on the load distribution behavior amongst the girders. In addition, distribution factors, DF's, determined from the field data for both interior and exterior girders were compared to the distribution factors from the design calculations provided by VDOT, AASHTO SSHB (1996), and AASHTO LRFD (1994). Distribution factors are dimensionless values that are intended to simplify bridge design and evaluation processes by allowing three-dimensional system behavior to be evaluated using one-dimensional, beam line methods. In this research, the distribution factors pertain to bending moment distribution factors and not shear distribution factors.

The specifications do not actually address the use of approximate distribution factors for an aluminum isotropic bridge deck on steel girders; therefore, the system was assumed to behave similar to a reinforced concrete deck on steel girders. This assumption coincided with Matteo (1997) which states "since the deck has very similar stiffness characteristics in each of the two primary directions its System II bending behavior (between girders) is not unlike that of a concrete deck."

4.4.2 Measured Load Fractions

Load fractions were determined for stationary static Load Cases 1 and 2 and dynamic Load Cases 6, 7, 8, and 9 (Reference Section 3.5 for load case descriptions). The load fractions were determined to examine the effects of truck location, both transverse and longitudinal, on the load distribution behavior amongst the girders. Load fractions are defined in a manner consistent with Stallings et al (1996), and are taken as the ratio of mid-span bottom flange strain in a girder divided by the sum of the mid-span bottom flange strains in all the girders for a particular event. Load fractions were determined using the WIM bottom flange field data from Girders 1 through 4. "Moving average" mid

span deflection data from the deflectometers was also used to determine load fractions in a similar manner. As previously mentioned a “moving average of six” was applied to data collected from the deflectometers in Test Set 2 to rid of constant, electronic signal noise.

Two types of load fractions were determined, “time response” load fractions and “max response” load fractions. This approach was also consistent with Stallings et al (1996). “Time response” load fractions were defined as load fractions calculated on a continual basis; thus each girder’s load fraction was calculated at the same time. “Max response” load fractions were defined using the maximum response recorded in each girder for a particular truck crossing. In the “max response” load fractions the maximum response in each girder may not have occurred at the same instance of time. Time strains load fractions were determined for the dynamic load cases of Test Set 2, which were Load Cases 6, 7, 8, and 9. “Max strains” load fractions were calculated for Load Cases 1, 2, 6, 7, 8, and 9. The same approaches were used to determine load fractions based on mid span deflection data obtained from the deflectometers on Girders 1 through 4.

4.4.3 Distribution Factors from Field Data

Distribution factors for the girders were determined from the field data to compare to the distribution factors from the design calculations of the Little Buffalo Creek Bridge and the approximate methods specified by AASHTO SSHB (1996) and AASHTO LRFD (1994). Distribution factors were determined for Load Cases 1, 2, 6, 7, 8, and 9 (Reference Section 3.5 for load case descriptions). The measured distribution factors were determined in a manner similar to the load fractions by using strain ratios of data obtained from mid-span WIM bottom flange gauges on Girders 1 through 4. The following equation was used to determine the distribution factor, DF, for the *i*th girder:

$$DF_i = \frac{n\varepsilon_i}{\sum_{j=1}^{k} \varepsilon_j} \qquad (4.1)$$

where ε_i = bottom flange strain at the *i*th girder; *k* = number of girders; and *n* = the number of side-by-side trucks. The above equation does not take into account the possible difference in girder section modulus values, which is consistent with Ghosn et al (1986) and Kim and Nowak (1997). An equation similar to Equation 4.1 was also used to calculate distribution factors using "moving average" mid span deflection data from the four girders. The strain values in the equation above were replaced with the deflection values to determine the distribution factors.

Several researchers in the past, O'Connor and Pritchard (1985) and Stallings and Yoo (1993) have used a "weighted strain" ratio to account for the differences in section modulus values of interior and exterior girders. The reason for using a weighted strain ratio was to account for the edge stiffening effect of secondary elements, such as curbs. If the concrete parapet is considered in the calculation of the transformed section properties of the exterior girder, then the bottom flange section modulus, S_b, increases to nearly 1830 in^3, which is nearly three times larger than the value of 621 in^3 determined if the parapet is excluded. The ratio of exterior girder section modulus, including concrete parapet, to that of an interior girder (S_b =624 in^3) would also increase to nearly three. Although the concrete parapet on the Little Buffalo Creek Bridge may provide some edge stiffening, it seems illogical to consider the parapet as acting full composite with the exterior girder.

4.4.4 "Lever Method" for Determining Distribution Factors

The "lever method" is discussed first because this was the approach used in the design calculations, and it is embedded in the AASHTO specifications' procedures. The "lever method" involves the assumption that the deck acts as a simply supported beam between the girders. Hinges are assumed at the location of all girders when determining the distribution factors for an interior girder. When determining the distribution factor for an exterior girder, the hinge is assumed to be located at the first interior girder and not the exterior girder, and thus the exterior girder and deck are a continuous section. The "lever method" is inherently conservative because the load is not allowed to distribute to

girders not supporting a loaded span because of the existence of the assumed hinges. Figures 4.5a and 4.5b show the locations of assumed hinges for both cases mentioned above.

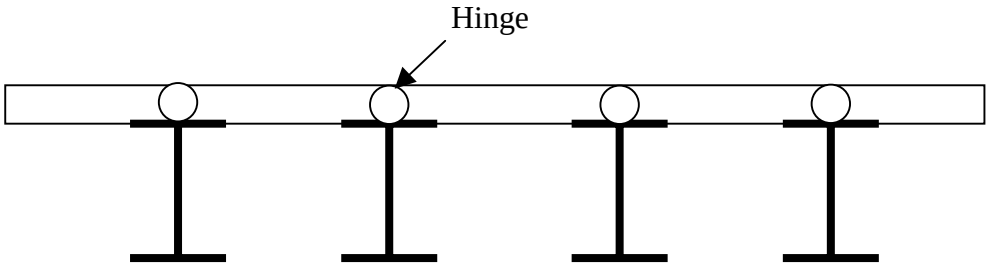

(a)

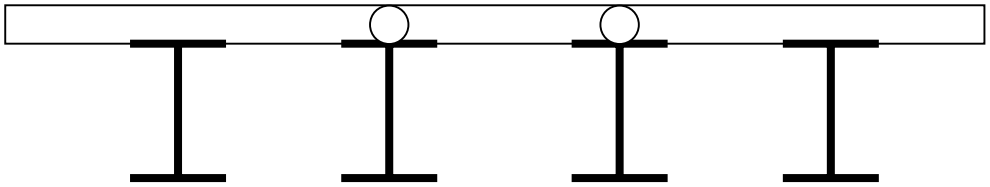

(b)

Figure 4.5 "Lever Method" Hinge Locations for Determining Distribution Factors: (a) Interior Girders, and (b) Exterior Girders

The design calculations provided by VDOT employed the "lever method" for both interior and exterior girder distribution factors (Reference Appendix B p. 153-155).

4.4.5 AASHTO SSHB (1996) Load Distribution Procedure

AASHTO SSHB (1996) specifies that no longitudinal distribution of loads can be assumed in determining the live load bending moments present in the longitudinal supporting members. It is assumed that all loads are transferred laterally, and the lateral distribution of live load moments in girders involves the use of a wheel load distribution factor for bridges designed for one traffic lane and for two or more traffic lanes. The

wheel load distribution factor is defined for various types of bridges depending on the floor type, supporting members, and number of loaded lanes. As previously mentioned, the aluminum deck was assumed to behave similar to a concrete deck; therefore, the wheel load distribution factors for a concrete deck on steel I-beams were used. The procedure for interior girders is presented first, followed by that for exterior girders. Wheel-load distribution factors are appropriate for use with one wheel-line of a truck, and therefore must be divided in half to be applicable to an entire truck or lane. It is noted that multiple presence is not included in the calculation of the wheel-load distribution factors.

4.4.5.1 Interior Girder Distribution Factors

AASHTO SSHB (1996) utilizes the following simplified equation for determining the wheel load distribution factor, *WDF*, for interior girders:

$$WDF = \frac{S}{D} \tag{4.2}$$

where S = girder spacing (ft); and D = a constant varying with the type of bridge floor, supporting members, and number of loaded lanes. For a concrete deck on steel I-beams with one traffic lane loaded, D has a value of 7.0. For two or more traffic lanes loaded the D value decreases to 5.5. The above equation is limited to systems with girder spacing, S, less than 10 ft for one traffic lane loaded and 14 ft for two traffic lanes loaded. AASHTO SSHB (1996) specifies that if the girder spacing requirements are not meet, then the “lever method” should be used.

4.4.5.2 Exterior Girder Distribution Factors

According to Section 3.23.2.3 of AASHTO SSHB (1996) the live load bending moment for exterior girders shall be determined by applying to the exterior girder the reaction of the wheel load obtained by assuming the floor to act as a simple span between

girders. This section specifies the use of the "lever method" for determining the exterior girders' distribution factors.

In addition, two separate guidelines are specified for the distribution of live load to exterior girders. First, the exterior girder shall not have less carrying capacity than an interior girder. This limits the distribution factor to at least the value obtained for the interior girders. Second, in the case of a concrete deck supported by four or more steel girders, the wheel load distribution factor for an exterior girder shall not be taken less than the following equation for values of *S* between 6 ft and 14 ft:

$$WDF = \frac{S}{4.0 + 0.25S} \tag{4.3}$$

where *S* = spacing between the exterior girder and adjacent interior girder (ft).

Appendix B (p. 156-158) contains calculations of the distribution factors for interior and exterior girders using AASHTO SSHB (1996).

4.4.6 AASHTO LRFD (1994) Load Distribution Procedure

The load distribution procedure in AASHTO LRFD (1994) allows for the use of simplified formulas to determine the lane fraction of live load moment to be applied to interior and exterior girders. The formulas are a result of the work performed by Zokaie et al (1991), and serve as a refinement of the methods used by the AASHTO SSHB. The researchers performed an extensive parametric study on bridges with varying material composition, cross-sectional geometry, and number of lanes loaded. The "lane fraction" term can be thought of as the distribution factor, DF, and is applicable to the effects of an entire truck. The formulas are for use with bridges with concrete decks and fairly regular geometry. According to ASSHTO LRFD (1994) Section 4.6.2.2.1, the following general conditions have to be met in addition to extra specific criteria for a particular bridge cross section type in order to utilize the formulas:

1) width of deck is constant,
2) unless otherwise specified, the number of beams is not less than four,

3) beams are parallel and have approximately the same stiffness,
4) unless otherwise specified, the roadway part of the overhang does not exceed 3.0 ft,
5) curvature in plan is less than the limit specified in Article 4.6.1.2 (For a bridge like the Little Buffalo Creek Bridge, with four beams and open girder cross sections , Article 4.6.1.2 limits the central angle subtended by each span to 3^o in order to neglect curvature in determining bending moments), and the
6) cross-section is consistent with one of the cross-sections in Table 1 (Table 1 lists the common deck superstructures covered by the distribution factor formulas, one of which is a typical concrete deck on steel girders).

The Little Buffalo Creek Bridge meets the above criteria except for the deck itself being made of concrete. As previously mentioned, for comparison purposes the deck was assumed to behave similar to a reinforced concrete deck. Additional specific limitations form ranges of applicability for using the formulas and are included in the following sections dealing solely with the interior and exterior girder distribution factors.

4.4.6.1 Interior Girder Distribution Factors

The interior girder distribution factors for a concrete deck on steel girders are defined for one design lane loaded and two or more design lanes loaded. The distribution factor for one-lane loaded is:

$$mDF = 0.06 + \left(\frac{S}{14}\right)^{0.4}\left(\frac{S}{L}\right)^{0.3}\left(\frac{K_g}{12.0Lt_s^3}\right)^{0.1} \quad (4.4)$$

The distribution factor for two or more lanes loaded is:

$$mDF = 0.075 + \left(\frac{S}{9.5}\right)^{0.6}\left(\frac{S}{L}\right)^{0.2}\left(\frac{K_g}{12.0Lt_s^3}\right)^{0.1} \quad (4.5)$$

where S = girder spacing (ft); L = girder length (ft); t_s = depth of concrete slab (in.); K_g = longitudinal stiffness parameter; and m = multiple presence factor. The multiple presence factors were included in the research conducted to develop the formulas, and therefore

are embedded in the distribution factor results. For comparison purposes, the multiple presence factor was removed from the one-lane loaded value obtained from the above equation by dividing by *m*. The multiple presence factor for one-lane loaded is 1.2. The multiple presence factor for two lanes loaded is 1.0, thus the value of *mDF* equals the distribution factor, DF. The longitudinal stiffness parameter, K_g, is determined from the following equation:

$$K_g = n\left(I + Ae_g^2\right) \tag{4.6}$$

where n = modular ration between the girder and the deck materials; I = moment of inertia of the girder (in^4); A = cross-sectional area of the steel girder (in^2)and e_g = vertical distance between the center of gravity of the basic girder and deck (in.). The modular ratio is the only numerical value in the distribution factor formulas that is material dependent. Although the aluminum deck was assumed to behave similar to a concrete deck, the modulus of elasticity of 6063-T6 aluminum (E_{Al} = 10100 ksi) was used to determine the modular ratio.

AASHTO LRFD (1994) sets a range of applicability for the formulas above by setting limits on the girder spacing, slab thickness, span length, and number of girders. The girder spacing, S, must be between 3-1/2 ft and 16 ft and the slab thickness, t_s, must be between 4-1/2 in. and 12 in. The span length, L, is limited to distances between 20 ft and 240 ft, and the number of girders must be at least four.

4.4.6.2 Exterior Girder Distribution Factors

The exterior girder distribution factors determined for a concrete deck on steel girders using the formulas specified in the tables of AASHTO LRFD (1994) are also for one lane loaded and two or more lanes loaded. The one lane loaded case specifies the use of the "lever method" for determining the exterior girder distribution factor. The specification notes that the multiple presence factor is not included in the "lever method." The multiple presence factor must be included for design; however, for comparison to the

data obtained from the testing with one truck in a lane at a time, the multiple presence factor was not included.

For two or more lanes loaded the approach is to use a correction factor, *e*, multiplied by the distribution factor determined for an interior girder. The correction factor, *e*, is specified as:

$$e = 0.77 + \frac{d_e}{9.1} \geq 1.0 \qquad (4.7)$$

where d_e = distance between the center of the exterior girder and the interior edge of the curb or traffic barrier (ft). The valued of d_e must be between –1 ft and 5-1/2 ft for the above formula to be utilized. A positive value of d_e corresponds to the exterior girder web being inboard of the interior edge of the traffic barrier and a negative value corresponds to an outboard location. The value of *e* must be greater than unity, which in essence limits the distribution factor for an exterior girder with two or more lanes loaded to at least the value calculated for an interior girder. This requirement matches that of AASHTO SSHB (1996). As previously mentioned, the multiple presence factor for two-lanes loaded is unity and thus the value of *mDF* is the value of the distribution factor, *DF*.

In addition, there is an interim provision that sets a lower bound on the exterior girder distribution factor in beam-slab bridge cross-sections that have cross-frames or diaphragms. The simplified formulas were derived from research on bridges that had interior, end diaphragms only. The Little Buffalo Creek Bridge has diaphragms between all the girders at the ends and at the third points of the bridge span. Section 4.6.2.2.2d of AASHTO LRFD (1994) states that the distribution factor for an exterior girder shall not be taken less than the value obtained by assuming the cross-section rotates and deflects as a rigid cross-section. The commentary gives the following equation:

$$R = \frac{N_L}{N_b} + \frac{X_{ext} \sum^{N_L} e}{\sum^{N_b} x^2} \qquad (4.8)$$

where R = reaction on the exterior girder in terms of lanes; N_L = number of loaded lanes under consideration; N_b = number of beams (girders); e = eccentricity of a lane from the center of gravity of the pattern of girders (ft); x = horizontal distance from the center of gravity of the pattern of girders to each girder (ft); and X_{ext} = horizontal distance from the center of gravity of the pattern of girders to the exterior girder (ft). For design, the multiple presence factors would need to be applied to the value of R. The R-values determined for the Little Buffalo Creek Bridge used the lane locations that would be used for design and not the off-center locations discussed in Section 3.5. The value of R is the same as the distribution factor, DF.

Appendix B (p. 159-161) contains calculations of the distribution factors for interior and exterior girders using AASHTO LRFD (1994).

4.5 Dynamic Load Allowance

4.5.1 Introduction

The dynamic load allowances for the girders of the Little Buffalo Creek Bridge were evaluated using the field data collected by VTRC. As mentioned in Section 2.2, dynamic load allowance refers to the increase above the static response that is a result of dynamic loading. Researchers in the past have completed analytical and experimental studies on a wide range of parameters that affect the dynamic load allowance. Parameters that affect the dynamic load allowance have been found to include the first natural frequency of the bridge, bridge continuity, the first natural frequency of the vehicle, vehicle suspension, vehicle axle configuration and weight, vehicle speed, roadway profile and roughness, and the existence of secondary stiffening elements such as curbs or parapets. The extent of the evaluation in this research is to gain through the available field data an insight on the behavior of the Little Buffalo Creek Bridge in regards to the

dynamic load allowance for the girders. The evaluation involves data from tests conducted with one type of vehicle (three-axle test trucks) and is not intended to provide a final conclusion on a precise dynamic load allowance for use in evaluating or rating the Little Buffalo Creek Bridge.

The dynamic load allowance values determined from the field data are compared to the values specified by AASTHO SSHB (1996), which was the specification used to determine the impact allowance during the design of the Little Buffalo Creek Bridge, and AASHTO LRFD (1994).

4.5.2 Influence Zone for Pertinent Field Data

Past researchers (Cantieni 1983, Bakht and Pinjarkar 1989, Paultre et al 1992, Stallings and Yoo 1993, Kim and Nowak 1997) have discussed or shown that the magnitude of dynamic amplification of responses can vary amongst the longitudinal supporting members in a bridge system. The researchers have concluded that improper interpretation of test data can lead to extreme overestimation of dynamic load allowances. It has been shown that girders with low static strains as a result of being away from the point of load application often show dynamic load allowance values that are extremely high. Dynamic load allowances determined from these girders tend to sway the results and do not provide an accurate measure of the appropriate dynamic load allowance. The dynamic load allowances should be determined from the girders with maximum static responses in order to comply with the current design code method of using the largest distribution factor multiplied by an impact factor for longitudinal supporting member design (Kim and Nowak, 1997).

Based on the need to include only pertinent data in the evaluation of the dynamic load allowance, Bakht and Pinjarkar (1989) and Paultre et al (1992) refer to an influence zone for proper instrumentation of a bridge to obtain the dynamic load allowance. The influence zone concept stemmed from research by Cantieni (1983). The transverse location of the vehicle on the bridge, the vehicle width, the bridge cross-section depth, and the point of reference for instrumentation are used to define the influence zone.

Figure 4.6 shows the influence zone and the associated parameters used to define the influence zone.

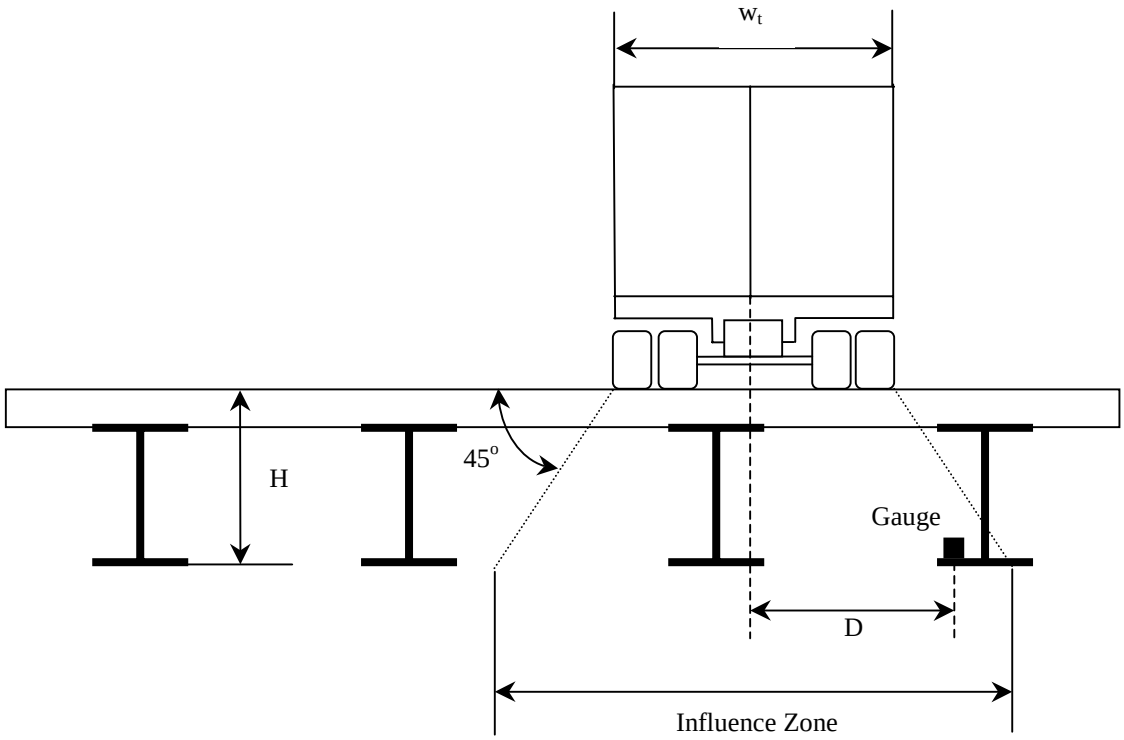

Figure 4.6 Influence Zone for Determining Dynamic Load Allowance

The following equation is used to determine the dimensionless value, α:

$$\alpha = \frac{D}{H + 0.5 w_t} \tag{4.9}$$

where D = distance between the instrumented location and the driving axis; H = height of the cross-section at the instrumented location; and w_t = truck width. The value of α must be less than or equal to unity to lie within the influence zone. Instrumented locations within the influence zone are considered to contain pertinent data for evaluation of the dynamic load allowance. According to Bakht and Pinjarkar (1989) the zone of influence

is affected by the transverse load distribution behavior of the bridge and thus the researchers suggested evaluating the dynamic load allowance for the girder with the highest static strain from the particular truck crossing.

In addition, Bakht and Pinjarkar (1989) suggested that the dynamic load allowance be evaluated for vehicles that are in the weight class of the design or evaluation vehicle. In this research on the Little Buffalo Creek Bridge, test trucks were used throughout the data collection processes; therefore, the test trucks were compared to the design truck using the maximum statically applied mid span moment of each truck from an influence line analysis as the comparison value. As discussed in Section 3.3 and shown in Table 3.3, the test trucks have weights and axle configurations that cause approximately 90 percent of the maximum static bending moment of the HS20-44 design truck. Ninety-percent of the maximum strain caused by the design or evaluation vehicle was set as the lower bound by Bakht and Pinjarkar (1989) for determining if normal traffic data is pertinent to the evaluation of the dynamic load allowance.

Bakht and Pinjarkar (1989) state that under similar conditions, dynamic amplification factors (dynamic load allowance) determined from deflection measurements are always greater than identical factors determined from strain measurements, and thus recommend the use of strain data. In this research, the dynamic load allowance was determined from deflections and strains to allow for comparisons between the two approaches.

One of the most varied aspects of evaluating dynamic load allowance from actual test data is the approach used to obtain the static response. Researchers such as Stallings and Yoo (1993) have used stationary truck test results to serve as the static response. Recent tests have used filtered dynamic data to obtain the equivalent static response from normal truck traffic (Billing 1984, Nassif and Nowak 1995, Kim and Nowak 1997). Paultre et al (1992) warned of the use of filtered data for short span bridges less than 15 m (≅ 50 ft) because the static frequency becomes equal to and possible higher than the first vibration mode of the bridge, which affects the filtering process. Paultre et al (1992) suggested the use of quasi-static (pseudo-static) testing to verify the static response from

the filtered dynamic response. In this research, VTRC performed pseudo-static tests of the Little Buffalo Creek Bridge in Test Set 3 using Truck 3. In lieu of filtering and because normal traffic data was not collected, the pseudo-static field data from the passage of Truck 3 was used as the static response of the bridge.

4.5.3 Dynamic Load Allowances from Field Data

The dynamic load allowances were evaluated from the WIM bottom flange strains and mid span deflections recorded for Girders 1 and 2 from Load Cases 6 and 7 and all load cases in Test Set 3 (Reference Section 3.5). In Test Set 3, the only girders instrumented by VTRC with WIM gauges and mid span deflectometers were Girders 1 and 2. Table 4.4 shows the resulting values from Equation 4.9 for the girders using the centerline of each girder as the point of instrumentation and the transverse truck location shown in Figure 3.13c. The value H is approximately equal to 3.90 ft for each girder of the Little Buffalo Creek Bridge and the width of the truck is 7.75 ft as shown in Figure 3.9 and Table 3.2.

Table 4.4 Influence Zone Parameter for Each Girder

Influence Zone Parameter				
	Girder 1*	Girder 2*	Girder 3*	Girder 4*
D (ft)	7	8	10	18
α	0.90	0.13	1.29	2.32

* H = 3.90 ft and w_t = 7.75 ft for all cases.

From Table 4.4 it can be seen that Girders 1 and 2 are the only girders that lie within the influence zone for determining the dynamic load allowance. The WIM strain and mid-span deflection values from Load Cases 6 and 7 were obtained using a different truck (Truck 1) than the load cases in Test Set 3 (Truck 3). However, the two trucks had the same axle configurations and widths, and differed in weight by only 160 pounds. The original mid-span deflection data from Load Cases 6 and 7 was used in the dynamic load allowance evaluation to be consistent with the load cases in Test Set 3. It is noted that

Girders 1 and 2 were the most heavily loaded girders in Load Cases 6 and 7, and the "moving average" deflection data differed from the original data by less than six-percent for these two girders. The use of original data allowed for any type of vibratory load resulting from vehicle-bridge interaction to be accounted for.

Dynamic load allowance in this research is denoted by the symbol, IM, and the following equation was used to obtain IM from the field data collected by VTRC:

$$IM = \frac{\varepsilon_{dyn} - \varepsilon_{stat}}{\varepsilon_{stat}} \tag{4.10}$$

where ε_{dyn} = maximum strain from dynamic loading of the bridge; ε_{stat} = maximum strain from pseudo-static loading of the bridge. In Equation 4.10, the maximum strains (ε_{dyn} and ε_{stat}) do not necessarily occur at the same time, thus the truck may not be in the same location longitudinally on the bridge for each girders' maximum strain. Equation 4.10 was used in a similar fashion to calculate dynamic load allowances from mid-span deflection data, and the maximum strain values were replaced with deflection values.

4.5.4 AASHTO Specifications' Procedures for Dynamic Load Allowance

4.5.4.1 AASHTO SSHB (1996) Procedures

Section 3.8 of AASHTO SSHB (1996) specifies the increase of highway live loads for elements of the superstructure to account for dynamic, vibratory, and impact effects. The Little Buffalo Creek Bridge has steel girders as the longitudinal supporting members of the superstructure, and thus the girders are subject to the specified increase. AASHTO SSHB (1996) impact allowance (I) is taken as a fraction of the live load stress and is determined from the following formula:

$$I = \frac{50}{L + 125} \tag{4.11}$$

where I = impact fraction with a maximum of 0.30; L = length of the portion of the span that is loaded to produce the maximum stress in the member (ft). The length L is the defined for various conditions (i.e., cantilever spans, continuous spans), but for a simply supported span like the Little Buffalo Creek Bridge, L is the span length. The value (1+I) would be applied to the live load moment in the girder during design to account for the increase in stress above the static applied live load moment in the girder. The value I is comparable to the dynamic load allowance (IM).

4.5.4.2 AASHTO LRFD (1994) Procedures

AASHTO LRFD (1994) Section 3.6.2 specifies that the static effects of the design truck or tandem, other than centrifugal and braking forces, shall be increased by the specified dynamic load allowance. The dynamic load allowance for members, such as supporting steel girders, in limit states other than fatigue and fracture is given as IM = 0.33. The dynamic load allowance is not applied to pedestrian loads or to the design lane load portion of the HL-93 live load model. The value (1+IM) would be the factor applied to the live load moments during design of the girders. Other cases are listed for exclusion of the dynamic load allowance, and for possible reduction of the dynamic load allowance, but are not applicable to the scope of this research.

4.6 Evaluation of Deck Stresses

4.6.1 Introduction

The deck stresses developed during the load tests were evaluated for two basic purposes. First, the deck stress ranges at different locations were evaluated to provide insight on how the ranges compared to the design allowable fatigue stress ranges for different detail categories. The specifications used for determining the design stress ranges were AASHTO SSHB (1996) in combination with the Specifications for Aluminum Structures-Allowable Stress Design from the Aluminum Design Manual (Aluminum Association 1994). Section 11 of AASHTO SSHB (1996) titled “Aluminum Design” refers to the Specifications for Aluminum Structures to provide a guide for

designers of aluminum bridges and other structural components. Load and Resistance Factor Design Specifications are provided in a separate Specifications for Aluminum Structures from the Aluminum Design Manual, but are applicable only to building-type structural members. For ease of referencing the Specifications for Aluminum Structures-Allowable Stress Design will be denoted as SAS-ASD (1994). AASHTO LRFD (1994) was also used to determine the design fatigue stress ranges for the different detail categories for comparison to the deck stress ranges from field data.

As mentioned in Section 3.4.2, VTRC placed transverse (TS) and longitudinal (LS) deck gauges at various locations at mid span of the Little Buffalo Creek Bridge (Reference Figure 3.12). The deck gauges were located at sites that were entirely base metal and at sites that were adjacent to longitudinal groove welds. The TS and LS gauges measured strains orthogonal and parallel to the axis of the groove welds, respectively, thus the difference in detail categories. The detail categories considered are discussed in the upcoming sections.

Second, the stresses located on opposite sides of the longitudinal, mechanical deck splice between Girders 1 and 2 were evaluated to determine if any significant stress discontinuities developed across the splice. The exact deck gauges used to evaluate the deck splice are included in the following section.

The extent of the evaluations of the deck stresses for the purposes previously mentioned are to gain through the available data an insight on the behavior of the deck and its details. The data collected was from a limited number of controlled tests with similar trucks and does not allow for a final conclusion on whether or not the deck is adequately designed for fatigue, or whether the mechanical splice is sufficient for all vehicular loadings.

4.6.2 Available Deck Gauges

VTRC did not connect every deck gauge during testing, and/or certain deck gauges were faulty at the time of the testing, thus data was not provided for every deck gauge. Table 4.5 lists each deck gauge and whether or not data was provided from the

test sets. Figure 3.12 and Table 3.4 provide more detailed information on the location of deck gauges and whether or not each deck gauge is located adjacent to a longitudinal groove weld.

Table 4.5 Available Deck Gauge Data

Test Set	Deck Gauge X= data provided											
	LS 1	LS 2	LS 3	LS 4	LS 5	TS 1	TS 2	TS 3	TS 4	TS 5	TS 6	TS 7
Test Set 1	X	X	X	X	X	X	X	X		X	X	X
Test Set 2		X	X	X	X	X	X	X		X	X	X
Test Set 3				X					X			

4.6.3 Fatigue Stress Range Evaluation Procedures

4.6.3.1 Determination of Detail Categories

Prior to evaluating the field data, the initial process was to categorize the different details within the deck adjacent to the deck gauges. The detail categories had to be established in order to determine the design S-N curves. Following Matteo et al (1996), the base metal of the deck was categorized as a Category A detail.

The detail category of the bottom panel, full-penetration, longitudinal groove weld between aluminum extrusions was not as obvious. The cross-section that results from the welding process (Reference Figure 3.5) does not exactly resemble any of the descriptive or illustrative examples provided by AASHTO LRFD (1994) or SAS-ASD (1994). Stresses at the longitudinal groove welds are both parallel and perpendicular to the weld axis, and are comprised of axial and bending stresses.

The commentary for SAS-ASD (1994) suggests the use of the fatigue strength of the standard detail that most closely approximates the new detail being designed. Considering the parallel and perpendicular loading as mutually independent, an attempt was made to categorize the longitudinal groove weld on the bottom of the deck with the illustrative examples and details that most closely resemble the actual welded connection.

For loading parallel to the longitudinal axis of the weld, Category B was considered to be the most appropriate detail category. The general condition, or construction, was considered to be similar to that of a "built-up member," and the detail category was based on the following description contained in SAS-ASD (1994):

> "Base metal and weld metal in members, without attachments, built-up of plates or shapes connected by continuous full or partial penetration groove welds…parallel to the direction of applied stress"

A similar description is present in AASHTO LRFD (1994).

For loading perpendicular to the longitudinal axis of the weld, the general "groove welded" condition was considered. Upon visiting the Little Buffalo Creek Bridge, the author noticed that the longitudinal welds on the bottom of the deck had not been ground flush, as was done for the top flange (Reference Section 2.8.2). Based on this observation and the following description from SAS-ASD (1994), Category C was considered to be the representative detail category for loading perpendicular to the longitudinal axis of the groove welds:

> "Base metal and weld metal at full-penetration groove welded splices…when reinforcement is not removed…"

A similar description is present in AASHTO LRFD (1994). The bead reinforcement present on the welds, which was not removed by grinding, is illustrated in Figure 2.2.

Although the longitudinal, mechanical deck splice would result in yet another detail category within the bridge susceptible to fatigue, this particular connection was not examined for fatigue considerations. The available deck gauges on each side of the mechanical splice are not actually located within the inner portion of the splice and thus do not provide data on the critical mechanical portions of the splice (i.e., shear block, fasteners).

4.6.3.2 Specifications' Fatigue Design Curves (S-N Curves)

The reader is referred to Section 2.8.3 for a discussion of S-N curves.

4.6.3.2.1 SAS-ASD (1994) Fatigue Design Curves

SAS-ASD (1994) considers both constant-amplitude loading and variable-amplitude loading for determining the allowable stress range for fatigue. Vehicular loading of a bridge is variable-amplitude loading, but the constant-amplitude fatigue limit is embedded in the fatigue stress check for variable-amplitude loading.

For variable amplitude loading, the design allowable stress range (S_{rd}) from SAS-ASD (1994) is given by the following equation:

$$S_{rd} = AN^{-1/m} \tag{4.12}$$

where N = the number of cycles to failure; and A and m are constants depending on the detail category. The constants are actually determined from the S-N curve for a particular detail category. For the detail under consideration, the constant A is the ordinate intercept of the log-log S-N curve for N = 1 cycle, and the constant m is the slope of the log-log S-N curve after 10^5 cycles. Table 4.6 presents the constants A and m from SAS-ASD (1994) for the detail categories considered in this research (Categories A, B, and C).

Table 4.6 S-N Curve Constants for Detail Categories in SAS-ASD (1994)

Constant	Detail Category		
	A	B	C
A (ksi)	96.5	130	278
m (ksi)	6.85	4.84	3.64

It is specified that the value of S_{rd} for a particular detail category shall not be greater than the upper bound value from Equation 4.12 when N equals 10^5 cycles. SAS-

ASD (1994) does not provide for fatigue strengths less than 10^5 cycles, which is approaching low-cycle fatigue. Low-cycle fatigue is more dependent on material strength (i.e., alloy and temper) and thus is not defined by the S-N curves for detail categories. For a specific detail category, the design allowable stress for variable-amplitude loading is the same as for constant-amplitude for values of N between 10^5 and $5x10^6$ cycles.

The major difference between the two types of loading involves the use of the fatigue limit. The fatigue limit (lower bound) is defined for constant-amplitude loading as the value of S_{rd} for N equal to $5x10^6$ cycles. There is no lower bound on the value of S_{rd} for variable amplitude loading because cracks can initiate at higher levels of stress and then propagate at stress levels well below the fatigue limit. However, SAS-ASD (1994) states that if the maximum stress range in a spectrum of loads is less than the fatigue limit then no further fatigue assessment is necessary. In essence, this statement takes into account the fact that if the maximum stress range in a spectrum is lower than the fatigue limit, then crack initiation should not occur. Figure 4.7, following this section, shows the schematic fatigue curves that result from Equation 4.12 for Categories A, B, and C for cycles above the upper bound limit.

If the maximum stress range in a spectrum of loads is greater than the fatigue limit, then an equivalent stress range must be calculated for comparison to the constant-amplitude allowable stress range (S_{rd}). The equivalent stress range, S_{re}, is derived from Miner's law (Reference Section 2.8.3.4) and is determined using the following equation:

$$S_{re} = \left(\sum_{i=1}^{N_s} \alpha_i S_{ri} \right)^{1/m} \tag{4.13}$$

where S_{ri} = the ith stress range in the spectrum; α_i = number of cycles in the spectrum of the ith stress range divided by the total number of cycles in the spectrum; N_s = number of stress ranges in the spectrum, and m was previously defined (SAS-ASD 1994).

The commentary to SAS-ASD (1994) notes that the stress ranges in a spectrum are difficult to determine unless cycle counting procedures are employed. Cycle counting

can be accomplished by determining an equivalent number of cycles for the primary stress range (Schilling 1984) or by "rainflow" cycle counting. The "rainflow" counting method is the most common and is basically a method of counting the number of cycle occurrences of a particular magnitude of stress range within a complex stress spectrum. The reader is referred to Sharp et al (1996) for additional information on "rainflow" cycle counting. The testing of the Little Buffalo Creek Bridge involved a small number of truck crossings; therefore, cycle counting was not employed.

SAS-ASD (1994) is not specifically a bridge design code, thus no assistance is provided concerning the number of cycles to consider for fatigue loading of the bridge. In the design calculations, the number of cycles was taken as two million. This value was determined using AASHTO SSHB (1996) Table 10.3.2A for transverse members and an assumed Average Daily Truck Traffic (ADTT) of 100. For a major highway with ADTT less than 2500, Table 10.3.2A specifies the use of 2 million stress cycles from truck loading.

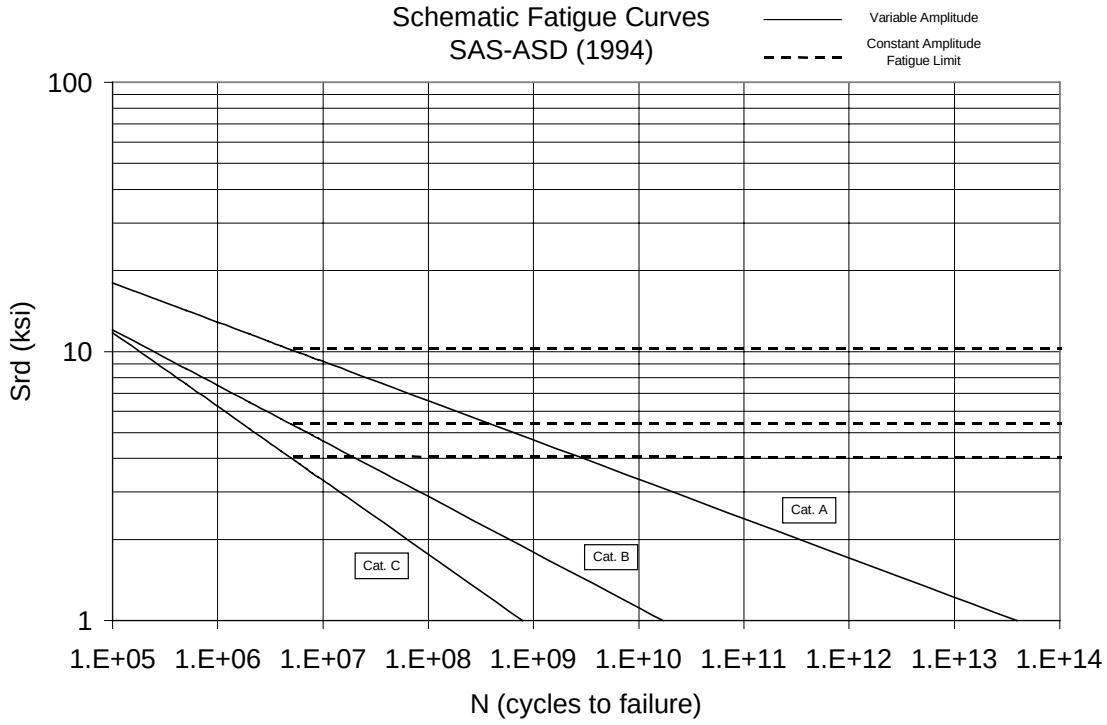

Figure 4.7 Schematic Fatigue Curves from SAS-ASD (1994)

4.6.3.2.2. AASHTO LRFD (1994) Fatigue Design Curves

AASHTO LRFD (1994) characterizes fatigue in two separate categories; distortion-induced fatigue and load-induced fatigue. Distortion-induced fatigue involves fatigue of components as a result of restricted movements. Barker and Puckett (1997) list the connection of transverse diaphragms to girder webs through connection plates as a possible detail susceptible to fatigue. AASHTO LRFD (1994) notes that distortion induced stresses are extremely hard to quantify by routine calculations, and thus suggest dealing with the phenomenon by adequate detailing. Distortion-induced fatigue is not evaluated in this research.

Load-induced fatigue is the fatigue of a detail caused by repetitive application of live load. AASHTO LRFD (1994) uses the stress based design approach and thus does not include residual stresses in the stress range. The specification states the provisions shall only be applied to details subject to a net applied tensile stress. AASHTO LRFD (1994) states that fatigue need not be considered if a detail is subjected to permanent

loading that results in compressive stresses that are twice the maximum tensile live load stress resulting from the application of the specified fatigue load combination. The specified fatigue load combination is not significant to this research, and thus is not discussed. In this research, the possible existence of compressive stresses in the deck due to permanent load is ignored, and each gauged detail is considered to be susceptible to fatigue.

The AASHTO LRFD (1994) approach to defining nominal fatigue resistance specified for a specific detail category of aluminum is similar to that of SAS-ASD (1994). The following equation is used to determine the nominal fatigue resistance, $(\Delta F)_n$:

$$(\Delta F)_n = \left(\frac{C_1}{N}\right)^{C_2} \geq \frac{1}{2}(\Delta F)_{TH} \qquad (4.14)$$

where N = number of stress-range cycles; C_1 and C_2 are constants depending on the detail category; and $(\Delta F)_{TH}$ = constant-amplitude fatigue threshold (fatigue limit) for the detail category. C_1, C_2, and $(\Delta F)_{TH}$ are listed in Table 4.7 for the detail categories considered in this research (Categories A, B, and C). The finite life portion of the right side of Equation 4.14 differs from that of Equation 4.12 in that the entire finite life expression of Equation 4.14 has an exponential power. The difference is accounted for by the increased value of C_1 as compared to the value of A used in SAS-ASD (1994). Equation 4.14 also plots as a straight line S-N curve on a log-log scale.

Table 4.7 S-N Curve Constants for Detail Categories in AASHTO LRFD (1994)

Constant	Detail Category		
	A	B	C
C_1 ($x10^8$)	100000	520	36
C_2	0.155	0.211	0.237
(ΔF_{TH}) ksi	9.5	6	4

The infinite life portion of the right hand side of Equation 4.14 is based on one-half of the constant-amplitude fatigue threshold, $(\Delta F)_{TH}$. Commentary in AASHTO LRFD (1994) concerning this limit states that the maximum stress range is assumed to be twice the live load stress range cause by the passage of the specified fatigue load combination. Barker and Puckett (1997) provide an additional explanation that clarifies the expression. Barker and Puckett (1997) state that the fatigue limit was lowered by 50 percent to account for the possibility of the heaviest truck in 75 years being twice the weight of the specified fatigue truck used in calculating the stress range during design. In this research the stress ranges are determined from the available field data, thus the fatigue truck is not discussed in detail.

Because AASHTO LRFD (1994) is a bridge design specification, assistance is provided concerning the determination of the number of stress-range cycles, *N*, to be used in Equation 4.14. The value of *N* is given as an expression that relates the number of cycles experienced by the bridge detail in a 75 year design life. The value of N is determined from the following equation:

$$N = (365)(75)n(ADTT)_{SL} \tag{4.15}$$

where n = number of stress-range cycles per truck passage; and $(ADTT)_{SL}$ = single-lane ADTT. The number of stress-range cycles is determined from Table 7.6.1.2.4-2 of AASHTO LRFD (1994) for transverse and longitudinal members. The value of n ranges from 1 to 2, and depends on the span length of the bridge and the spacing of the transverse members. Barker and Puckett (1997) state that values of n greater than unity are to account for additional vibration cycles that occur after the truck leaves the bridge. The value of n was taken as unity for the Little Buffalo Creek Bridge groove welds.

AASHTO LRFD (1994) considers the most heavily traveled lane in determining the value of N for use in Equation 4.15, thus the use of the single-lane ADTT. In lieu of site-specific traffic surveys that provide single-lane loaded traffic data, AASHTO LRFD

(1994) provides assistance in determining the $(ADTT)_{SL}$ from both the ADTT and the Average Daily Traffic (ADT). The method of determining $(ADTT)_{SL}$ from the ADTT is applicable to this research. AASHTO LRFD (1994) allows for the $(ADTT)_{SL}$ to be determined from ADTT by the following equation:

$$(ADTT)_{SL} = p(ADTT) \tag{4.16}$$

where p = the fraction of truck traffic in a single-lane. For the Little Buffalo Creek Bridge, which has two-lanes available to traffic, AASHTO LRFD (1994) specifies p to be taken as 0.85. The design calculations provided by VDOT contained two values of ADTT; an actual value (ADTT = 54) and a conservative design assumption (ADTT = 100).

The schematic fatigue curves for Categories A, B, and C are shown in Figure 4.8 following this section. The ordinate axis is the log of the nominal fatigue resistance, $(\Delta F)_N$ and the abscissa was taken as the log of the number of stress-range cycles, N. As for the fatigue schematics from SAS-ASD (1994), the entire curves are shown for values of N between 10^5 and 10^{14} cycles.

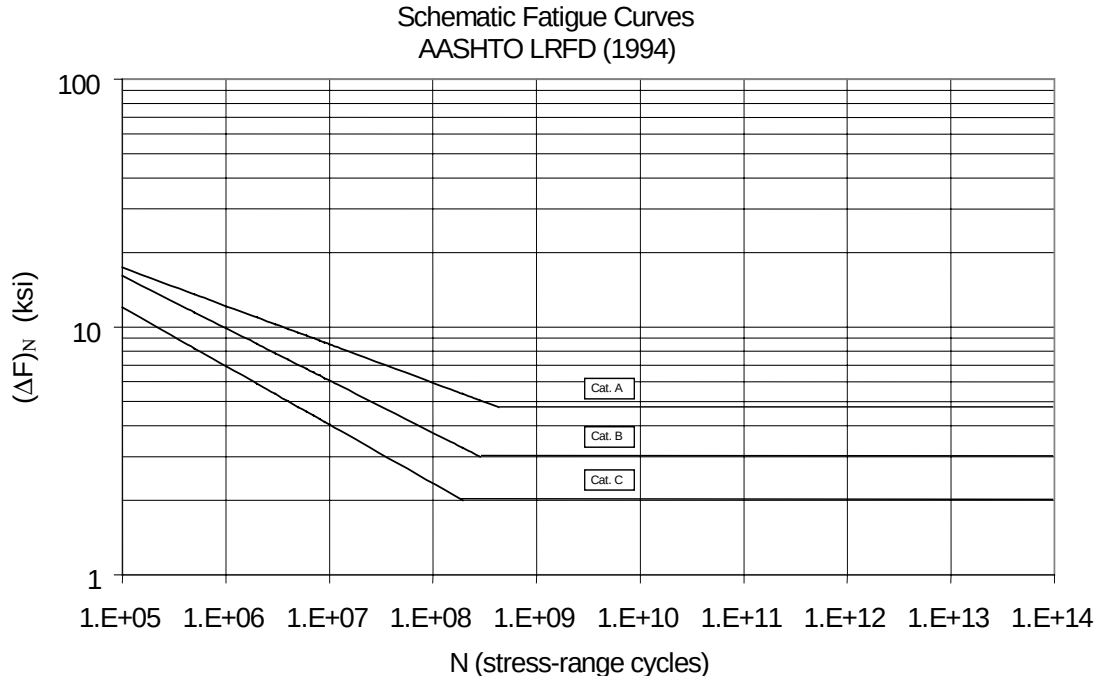

Figure 4.8 Schematic Fatigue Curves from AASHTO LRFD (1994)

4.6.3.3 Stress Ranges from Available Field Data

The absolute peak-to-peak strain (i.e., absolute value of the difference between maximum and minimum strain) was used to determine the strain range from each deck gauge. The stress ranges were calculated by multiplying the strain ranges by the modulus of elasticity of aluminum (E_{AL} = 10100 ksi). Stress ranges for Test Sets 2 and 3 were computed from the available continuous deck gauge data (Reference Table 4.5). It is noted that Load Cases PS-1 and PS-2 of Test Set 3 were pseudo-static load cases and thus not affected by impact. All field data from the deck gauges from Test Sets 2 and 3 was "moving average of six" data.

Two-lane loaded conditions were not obtained from superposition, as was done for the load distribution evaluation. In all probability, the deck would be affected by localized stresses (System III behavior) from the application of the load, and deck gauges closer to the tire locations would be affected accordingly. Superposition of one-lane loaded results for symmetrically placed gauges would not serve to account for the localized, System III behavior present in the deck.

The only available field data for multiple truck loading of the bridge was from Test Set 1. However, the field data from Test Set 1 did not allow for correct stress ranges to be calculated because of the nature of the testing process. Test Set 1 involved stationary static testing of the bridge at three pre-selected locations, thus data was collected for only three locations along the bridge span. In addition, stationary static testing negated the effect of impact on the deck stresses, whether additive or not. Therefore, the field data from Test Set 1 was used in a slightly different capacity. When the deck gauge showed both tensile and compressive strains then the stress range was calculated as previously explained. When the deck gauge showed only compressive or only tensile strains, then the stress range was determined from the absolute value of the largest strain magnitude. Once again, it is noted that stress ranges determined from the field data of Test Set 1 might not represent the true stress ranges developed in the deck.

4.6.4 Mechanical Deck Splice Evaluation Procedures

The mechanical deck splice was evaluated using deck gauges TS 4, TS 5, TS 6, and TS 7 (Reference Figure 3.12). Figure 4.9, following this section, shows the deck splice and the relative gauge locations with respect to the mechanical deck splice. The stress ranges experienced by the deck at the above gauge locations were evaluated to determine if any gross stress discontinuities existed across the splice. Table 4.5 shows that field data was not provide for TS 4 of Test Set 1, but was for TS 4 of Test Set 3. Various load cases in Test Sets 1 and 3 were with similar transverse truck locations and truck speeds (Reference Section 3.3). For the similar load cases, the field data from TS 4 of Test Set 3 was used in combination with the field data from TS 4 of Test Set 1.

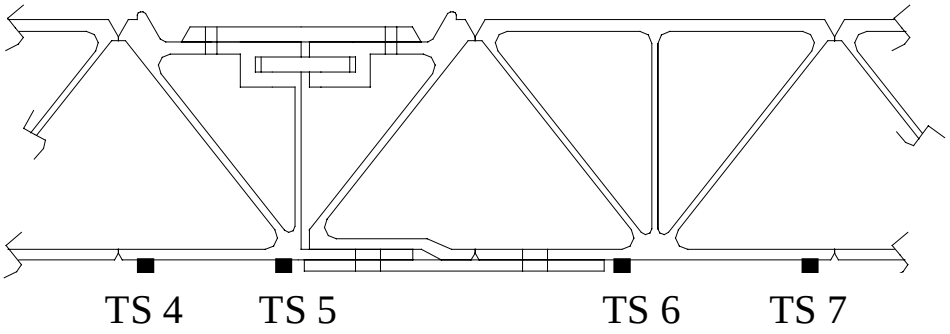

Figure 4.9 Transverse Deck Gauges Associated with the Mechanical Deck Splice Evaluation

4.7 Summary

The methods used to evaluate the field data have been presented for each research topic (composite action, load distribution, dynamic load allowance, and developed deck stresses). The methods presented in this chapter are referenced throughout the remainder of chapters discussing the results of the evaluations.